Nonlinear waves on circle networks with excitable nodes

Nonlinear waves on circle networks with excitable nodes

Shouwen Wang[1] **and Yueheng Lan**[2]

[1] Department of Engineering Physics, Tsinghua University, Beijing 100084,
People's Republic of China
[2] Department of Physics, Tsinghua University, Beijing 100084, People's Republic of China

E-mail: wang-sw09@mails.tsinghua.edu.cn and lanyh@mail.tsinghua.edu.cn

Abstract

In this paper, we propose a new model of the Kuramoto type to study nonlinear wave generation and propagation on a circle network with excitable node dynamics, and reveal certain common features of traveling wave solutions, which are independent of local dynamics but strongly related to the diffusive coupling of neighboring nodes. In view of the stability and size of the basin of attraction, regular nonlinear waves and, in the case of a large number of nodes, circulating pulses are the most important ones. The period T and the functional expression for regular nonlinear waves are computed analytically, which matches well with the numerical result. A new type of solution, the special nonlinear wave existing only for the discrete node dynamics, is studied and compared with the regular solution.

PACS numbers: 05.45.Xt, 47.54.Bd, 89.75.Kd

(Some figures may appear in colour only in the online journal)

1. Introduction

Synchronization is one type of collective and emergent behavior of coupled agents which involves spontaneous locking to a common oscillation frequency. Investigation of this ubiquitous and important phenomenon is intense and fruitful in recent years. Much progress has been made in diverse fields, including examples from networks of pacemaker cells in the heart [1, 2], metabolically synchronized yeast cells [3, 4], congregation of synchronously flashing fireflies [5, 6], arrays of diode lasers [7, 8] or microwave oscillators [9] and wired superconducting Josephson junctions [10]. It is probably one of the most studied phenomena of spontaneous emergence of rhythms in non-equilibrium systems. Various models have been proposed to investigate the different features of this emergent behavior, including its onset and stability, among which the Kuramoto model is the most widely used for its simplicity of formulation and elegance in analysis. The Kuramoto and similar models deal with coupled
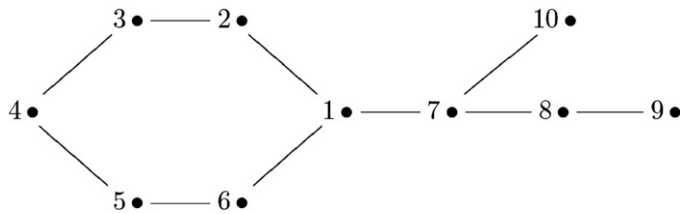
Figure 1. A simple example of a network with a circle sub-network.

oscillators and study how oscillation of individual members is shaped by coupling strength and topology. Other dynamical aspects, such as the impact of noise, finite-size effect and co-evolution of structure and dynamics, have also been explored [11, 12], together with disparate local dynamics [13] while much more remains to be probed [13].

The spatiotemporal pattern formation in excitable media has long been a hot topic for researchers in both applied and theoretical arenas. If the excitable dynamics is mounted on each node of a network, a discrete analogue of the excitable media is created, the collective dynamics of which critically depends on the network structure. Hu *et al* recently investigated the diffusively coupled Bär–Eiswirth model and found that different nonlinear waves may emerge spontaneously with a properly designed coupling strategy [14]. These nonlinear waves possess an interesting feature: the evolution on the neighboring nodes is equally separated in time. Based on comprehensive numerical computation results, they proposed a phase-advanced model which explains how all the nodes of the network are driven by a self-sustained central circle sub-network of oscillating nodes. Hence, a dynamically complex network can be viewed in a much simpler way: the central driving circle sub-network and the attached trees, which is determined by system dynamics. In figure 1, the nodes 1–6 make the circle sub-network and 7–10 are attached as a tree branch. Once a driving circle network is selected dynamically, the oscillation on it will determine the behavior of the rest of the network. Therefore, it is crucial to identify possible spatiotemporal patterns on a circle network of excitable nodes with diffusive coupling.

In fact, the propagation of nonlinear waves along a circular track of excitable media was observed experimentally in heart muscles long ago and has been well explained based on empirical physiology models [15, 16]. Similar waves were also observed in other low-dimensional systems, such as the charge density waves in the quasi 1D metals [17]. In all these studies, a plethora of wave patterns were explored and their existence and stability were investigated with different analytical or numerical tools. However, in their mathematical description, the sophisticated set of coupled nonlinear differential equations often prevent an analytic approach and thus hinder our full understanding of the wave dynamics even in simple cases. Based on the observed universal features of wave propagation on networks, we feel that it is possible and necessary to find a model which keeps the essential elements of those well-known models, such as the diffusively coupled Bär–Eiswirth model, but with a more simplified description in order to enable analytic manipulation.

Inspired by the success of the Kuramoto model in synchronization, here we propose a new model of similar type to target the problem of spatiotemporal pattern formation in a circle network with excitable node dynamics. We put a one-dimensional phase oscillator at each node, which is similar to the Kuramoto model but with nonuniform local frequency and diffusive coupling. The model is considerably simpler than the Bär–Eiswirth model used by Hu *et al* [14] but captures the key dynamics. Detailed studies on the circle network have been carried out, in which interesting spatiotemporal patterns are observed, compared and classified

analytically according to the solution in the limit of uniform local frequency. Among all the nonlinear waves, the regular nonlinear wave, characteristic of its equal-time-separation, is of great interest and significance. Further perturbation analysis indicates that the equal-time-separation solution is ubiquitous in systems with coupled excitable dynamics and that it is stable. The restitution and dispersion curves of this wave bear a remarkable similarity to those of a ring of excitable media, which implies the physical relevance of our model and its solutions. Other types of solutions, stable or unstable, are also found, including one special solution that seems to have no analogue in the continuum limit.

The equal-time-separation solution is related conceptually to the lag synchronization of two coupled nonidentical chaotic oscillators, in which physical observables of the two become synchronized but with a time lag [18]. However, in our model, identical excitable phase oscillators are coupled diffusively and thus both the formed patterns and the underlying interaction between agents are different. In celestial mechanics, a remotely related example is the choreographic solution for the *n*-body problem, in which the moving bodies are also separated by a constant time interval [19]. Henceforth, this equal-time-separation solution seems to be universally present and much work is needed to reveal its manifestation and implication in different contexts.

Our model is an over-damped version of the well-known Frenkel–Kontorova model [20–22], which has become one of the fundamental and universal descriptions of low-dimensional nonlinear physics. The classical Frenkel–Kontorova model describes a chain of classical particles evolving on the real line, coupled with their neighbors and subjected to a periodic potential. In the continuum limit, i.e., the distance a_0 between neighboring nodes satisfies $a_0 \ll 1$, the Frenkel–Kontorova model is reduced to the sine-Gordon equation, which is a completely integrable nonlinear partial differential equation. The simplicity of the Frenkel–Kontorova model, as well as its surprising richness of dynamics and capability to describe a range of important nonlinear phenomena has attracted a great deal of attention from researchers working in solid-state physics and nonlinear science, providing a unique framework to combine physical concepts and make analysis in a unified and consistent way. It is hoped that our simplified version of the Frenkel–Kontorova model also gives interesting insights into pattern formation in the context of complex networks.

The paper is organized as follows. In section 2, we motivate the introduction of our model, and a detailed discussion of its solution is given in section 3. In particular, the stability condition and periods of regular solutions are analyzed with a perturbation approach. The regular nonlinear wave turns out to be a generic pattern arising in circle networks with excitable node dynamics, which is discussed in detail in section 3.2. The relation of the circulating pulse in excitable media and the regular nonlinear wave is investigated in section 4 with the dispersion and restitution curves being plotted. We summarize our results in section 5.

2. The model

Much effort has been devoted to the study of nonlinear wave propagation or self-sustained oscillation on different types of networks. The Bär–Eiswirth model [23] recently used by Hu *et al* is written as

$$\frac{\mathrm{d}u_i}{\mathrm{d}t} = -\frac{1}{\epsilon} u_i (u_i - 1) \left(u_i - \frac{v_i + b}{a} \right) + \Delta^2 u_i, \tag{1a}$$

$$\frac{\mathrm{d}v_i}{\mathrm{d}t} = f(u_i) - v_i, \tag{1b}$$
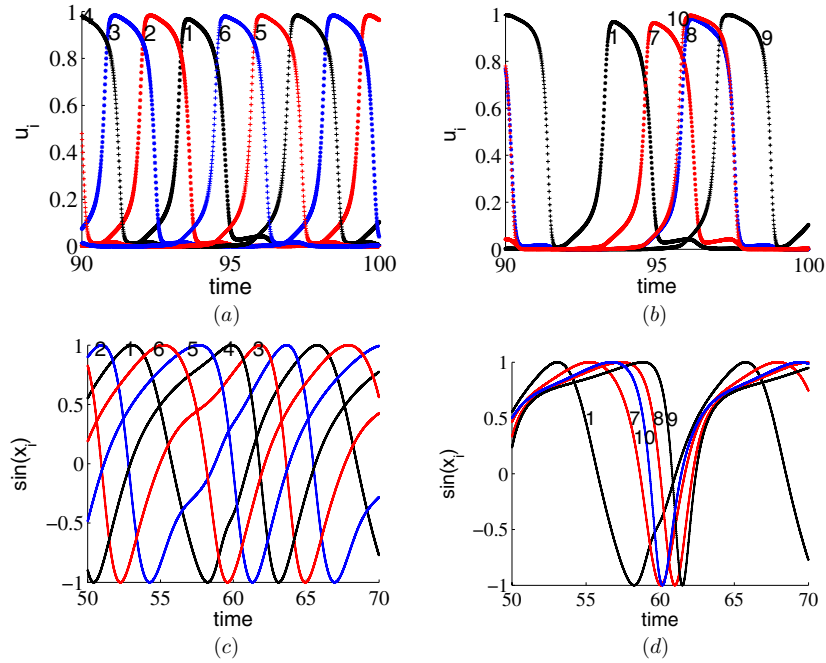
Figure 2. Nonlinear waves on the network shown in figure 1. (*a*), (*b*) Dynamics (i.e., $u_i(t)$, plotted as '*' or '+') of different nodes for equation (1) with $\epsilon = 0.04$, $b = 0.07$, $a = 0.84$, $d = 0.2$, for nodes (*a*) in the circle sub-network and (*b*) in the attached tree branch. (*c*), (*d*) Corresponding dynamics for equation (4) with $w = 0.8$, $\epsilon = 1$, $d = 1$, for nodes (*c*) in the circle sub-network and (*d*) in the branch. Note that the vertical coordinate for (*c*) and (*d*) is $\sin(x_i)$ so that the similarity between (*a*) (*b*) and (*c*) (*d*) is more obvious.

where

$$f(u) = \begin{cases} 0, & u < \frac{1}{3} \\ 1 - 6.75u(u-1)^2, & \frac{1}{3} \leqslant u \leqslant 1 \\ 1, & u > 1, \end{cases}$$

and Δ^2 denotes the discrete Laplacian, which can be defined on a bidirectional graph $D = \{V, E\}$ with the vertex set $V = \{v_1, v_2, \ldots, v_n\}$ and the edge set $E = \{e_1, e_2, \ldots, e_m\}$. With $a_{i,j}$ representing the number of edges from vertex v_i to vertex v_j, the discrete Laplacian is

$$\Delta^2 u_i = \sum_{j=1}^{n} a_{j,i}(u_j - u_i). \tag{2}$$

It was discovered that on a network of similar type to that in figure 1, with equation (1), the dominant phase-advanced driving (DPAD) mechanism [14] governs the dynamics. In figures 2(*a*) and (*b*), we show the dynamical behavior of all nodes of the network shown in figure 1. A circulating nonlinear wave is found on the circle sub-network with nearly uniform velocity, which indicates equal-time-separation between adjacent nodes. The small discrepancy is caused by the side branch attached. The dynamics of the nodes in the side branch is subordinate to that of node 1, as illustrated in figure 2(*b*). The DPAD mechanism, i.e., a cascading driving ladder relaying sustained oscillations, is vividly shown in figure 2(*b*). For example, node 7 is always pulled by node 1 away from the stable fixed point of the local dynamics. The circle sub-network plays an essential role in the current network dynamics

4

which motivates an in-depth investigation on possible dynamical behavior of a circle network with various local dynamics to explore general features of the wave propagation. Below, we will take one of the simplest cases, i.e., a particular one-dimensional equation, to model the local dynamics.

A general equation of motion with local 1D dynamics and nearest neighbor interaction along a circle network could be written as:

$$\dot{x}_i = f(x_i) + R(x_{i-1}, x_i, x_{i+1}), \quad i \in \{1, 2, 3, \ldots, n\}, \quad x_i \in \mathbb{R} \tag{3}$$

where $f(x_i)$ denotes the local dynamics and $R(x_{i-1}, x_i, x_{i+1})$ is the coupling term between neighboring nodes. The total number of nodes is assumed to be n and due to circle topology, $x_{i \pm n} = x_i$. The dynamics is invariant under the rotation $x_i \to x_{i+k}, \forall k \in \mathbb{N}$, the reflection $x_i \to x_{n+1-i}$ and their group composite. The periodicity also implies a simple composition rule. Suppose the variables $\{x_i(t)\}_{i=1,2,\ldots,p}$ and $\{y_i(t)\}_{i=1,2,\ldots,mp}$ describe dynamics governed by the same equation of motion (3) on two circle networks with p and mp nodes respectively. The identification $y_i = x_j$, for $i = j \pmod{p}$, $i = 1, 2, \ldots, mp$ will generate a solution for the y-system with any x-solution, as illustrated in figure 4. The dynamics in figure 4(*d*) is inherently a spatial juxtaposition of that in figure 4(*g*).

For simplicity, without loss of generality, we will mainly use the diffusion model below

$$\dot{x}_i = \omega - \epsilon \sin(x_i) + d \sin(\Delta^2 x_i), \quad i \in \{1, 2, 3, \ldots n\}, \quad x_i \in \mathbb{R} \tag{4}$$

where Δ^2 is the Laplacian operator, as defined in equation (2). For circle networks, $\Delta^2 x_i = x_{i+1} + x_{i-1} - 2x_i$. The local dynamics is identical to that of the Kuramoto model if $\epsilon = 0$. Besides, the case $\epsilon > \omega$ corresponds to the so-called theta–neuron model, also known as Ermentrout–Kopell model [24] and the case $\epsilon < \omega$ is widely investigated in the field of Josephson junctions [25]. When ϵ is greater than but close to ω, a stable and an unstable equilibrium coexist on the phase circle of the local dynamics, and the system becomes excitable: all the orbits go to the unique stable equilibrium unless a perturbation brings the state over the unstable one, which induces a large excursion. Compared to the usual two-dimensional excitable dynamics equation (1), the current one is much simpler so that a relatively thorough discussion of its solution becomes possible. In the continuum limit, the wavelength $\lambda \gg 1$ and $\Delta^2 x_i = x_{i+1} + x_{i-1} - 2x_i \ll 1$, so that $\sin(\Delta^2 x_i) \to \Delta^2 x_i$. Here, the wavelength λ is measured in terms of the number of nodes that are spanned with a spatial period of the wave. The term $\sin(\Delta^2 x_i)$ is invariant under a phase shift of $x_i \to x_i + 2k_i\pi, k_i \in \mathbb{Z}$.

With equation (4), the dynamical behavior of all nodes in figure 1 is displayed in figures 2(*c*) and (*d*). The dynamical behavior in figure 2(*c*) looks similar to that in figure 2(*a*). Hence, the simple one-dimensional equation (4) seems to have captured the essential features of the Bär–Eiswirth model (1), although the precise wave profiles are not identical. Here, we emphasize that although the interaction between the circle sub-network and the branch network is mutual, the DPAD mechanism governs the uni-directional propagation of action, as clearly seen in figure 2(*d*). The back reaction of the branch on the circle network is small, so the equal-time-separation profile is well preserved. For a general nonlinear wave propagation, this may not be the case. The observed DPAD structure is intimately related to the excitable node dynamics. Our model equation (4) captures well this particular feature of the dynamics.

The new model is closely related to the Frenkel–Kontorova model, which describes a harmonically coupled particle chain moving in a periodic potential. If ϕ denotes the position of the particle $i \in \mathbb{Z}$, one of the simplest Frenkel–Kontorova models could be written as

$$m\frac{\mathrm{d}^2\phi}{\mathrm{d}t^2} + \gamma\frac{\mathrm{d}\phi_i}{\mathrm{d}t} = L + \sin(\phi_i) + \Delta^2\phi_i,$$

where m is the particle mass, γ a friction coefficient and L a constant driving force. The term $\sin(\phi_i)$ is the force exerted by a periodic potential and the interaction $\Delta^2\phi_i = \phi_{i+1} + \phi_{i-1} - 2\phi_i$ is diffusive.

In the over-damped limit $m \ll \gamma = 1$, we neglect the inertial term and obtain

$$\frac{\mathrm{d}\phi_i}{\mathrm{d}t} = L + \sin(\phi_i) + \Delta^2\phi_i. \tag{5}$$

As an application, this simplified model reproduces the complex behavior of the charged density waves (CDWs), including the depinning transition, mode-locking and sub-threshold hysteresis [26–28], where the ϕ_i describe the configuration of the CDW. Our model, when implemented on circle networks, is equivalent to the over-damped Frenkel–Kontorova model in the continuum limit since $\sin(\Delta^2 x_i) \to \Delta^2 x_i$ in that limit.

Strogatz *et al* also used the model below to characterize the CDW on a ring [29],

$$\dot{\phi}_i = L - h\sin(\phi_i - \alpha_i) + \frac{K}{n}\sum_{j=1}^{n}\sin(\phi_j - \phi_i). \tag{6}$$

The main difference between equation (6) and our model equation (4) is that the coupling term in equation (6) is global rather than local as in our model.

To visualize the dynamical behavior of equation (4), it is convenient to denote the state of a node by a point on a circle (phase space of the local dynamics) and so the state of the whole system can be represented by a group of points on the same circle. If $d = 0$ in equation (4), then each point will move along the circle according to the local dynamics while for $d \neq 0$ the points will interact with their nearest neighbors. When $|w| < |\epsilon|$, the local dynamics have a unique stable fixed point while the interaction may push nodes away from this stable equilibrium. In fact, a threshold coupling exists which delimits regimes for a stable fixed configuration and for stable circulation along the circle, i.e., a stable nonlinear wave on the network. The simplicity of the model enables a detailed analysis of these oscillatory solutions as shown in next section.

3. Spatiotemporal patterns

Let us consider the equation below

$$\dot{x}_i = w + d\sin(x_{i+1} + x_{i-1} - 2x_i), \quad x_i \in \mathbb{R}, \tag{7}$$

which is the special case $\epsilon = 0$ of equation (4). In this simplified equation, a two-parameter continuous symmetry group comes into existence: the equation is invariant under $x_m \to x_m + c_1 + mc_2$, $\forall c_1, c_2 \in \mathbb{R}$. Of course, the boundary conditions should be satisfied under this transformation. For the periodic boundary condition, c_2 can only take discrete values. With the notation

$$\eta_i = \begin{cases} x_{i+1} - x_i, & i \in \{1, 2, \ldots, n-1\} \\ x_1 - x_n, & i = n, \end{cases}$$

equation (7) becomes

$$\frac{\mathrm{d}\eta_i}{\mathrm{d}t} = d\sin(\eta_{i+1} - \eta_i) - d\sin(\eta_i - \eta_{i-1}), \tag{8}$$

with the constraints $\sum_i^n \eta_i = 2k\pi$, $\eta_{n+1} = \eta_1 + 2p\pi$, $k, p \in \mathbb{Z}$ due to periodicity.

3.1. General solutions

Any stationary solution for equation (8) satisfies

$$\eta_{i+1} - \eta_i = \beta \quad \text{or} \quad \pi - \beta, \qquad \forall i, \tag{9}$$

where β is a constant chosen to satisfy the periodic boundary condition. So, the structure of the general solution is rather complex even for the simplified equation. If there exists j such that both choices of equation (9) are made, in the continuum limit, $\beta \to 0$, $\pi - \beta \to \pi$, the resulting solution does not correspond to physical reality, which hence only appears when the interacting units are discrete. Below is a simple case with an alternating choice of the two values

$$\eta_{2i} - \eta_{2i-1} = \beta, \quad \eta_{2i+1} - \eta_{2i} = \pi - \beta, \quad i \in 1, 2, \ldots, \quad \text{for} \quad n = 4m, \quad m \in \mathbb{N}.$$

We then have

$$\eta_2 = \eta_1 + \beta, \quad \eta_3 = \eta_1 + \pi, \quad \eta_4 = \eta_1 + \pi + \beta, \quad \text{and} \quad \eta_{i+4} = \eta_i + 2\pi,$$

where $\beta = k\pi/m$ satisfies the periodicity condition when we take $\eta_1 = 0$ for simplicity. Therefore,

$$x_2 = x_1, \quad x_3 = x_1 + \beta, \quad x_4 = x_1 + \pi + \beta \text{ and } x_i = x_{i-4} + 2\pi + 2\beta, \quad \text{for} \quad i > 4, \tag{10}$$

which is a rather complex wave on the circle network. Possible unstable nonlinear waves of this type are abundant, as illustrated in figure 3. For all solutions in figure 3, they are checked numerically to be unstable. However, a proof for the stability of a general solution does not seem to be easy.

In order to describe waves on a circle network, a triple-plot set is used throughout this paper, among which the first plot depicts the time course for each node, the second plot takes a snapshot of this dynamic wave and marks the profile in the phase space, and the third one displays the state of each node in the second plot. This protocol is demonstrated in figure 3.

A more interesting case satisfies $\eta_{i+1} - \eta_i = \beta$ invariably such that

$$\eta_i = \eta_1 + (i-1)\beta. \tag{11}$$

But with the periodicity condition following equation (8), we have the constraint

$$\beta = \frac{2p\pi}{n}, \quad \eta_1 = \frac{2k\pi - (n-1)p\pi}{n}. \tag{12}$$

The solution for the phase variable x_i is

$$x_i = (\omega + d\sin\beta)t + (i-1)\eta_1 + \frac{(i-1)(i-2)}{2}\beta + x_{00}, \tag{13}$$

where x_{00} is some arbitrary initial phase. The stability of this solution is discussed in appendix A. In section 3.3, we will discuss several special cases for this general solution when $\beta \neq 0$, which are stable for $d\cos\beta > 0$ according to appendix A and referred to as special solutions or special waves in the current paper.

When going to the continuum limit, only the solutions with $\beta = 0$ ($p = 0$) make physical sense so that the phase separations become equal, which is referred to as the regular solution or regular wave and will be further investigated in detail later. Under this condition equation (13) is much simplified:

$$x_i = \omega t + \frac{2(i-1)k\pi}{n} + x_{00}. \tag{14}$$

Note that the natural frequency is restored. According to appendix A, regular waves are stable. As we will see, the regular wave will persist even for $\epsilon \neq 0$, where the phase-space separations between the x_i are non-constant but their temporal separations remain constant.
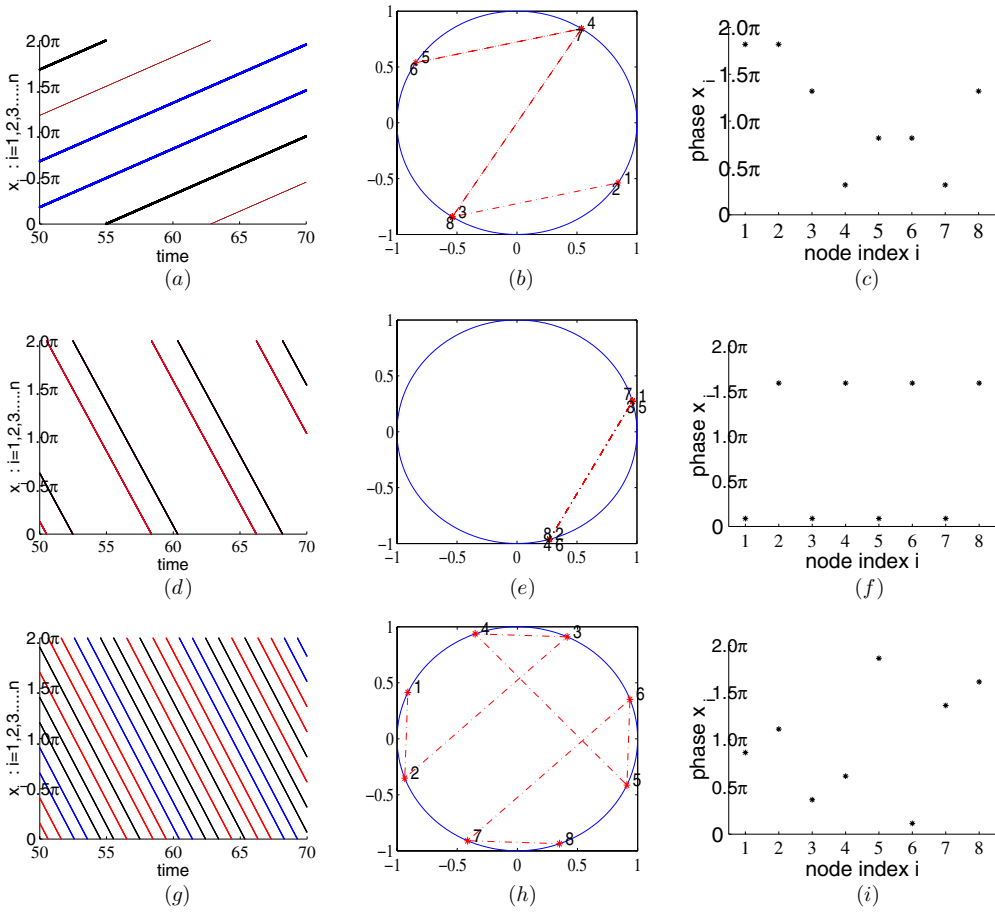
Figure 3. Some interesting unstable waves on the circle network with $n = 8$. (*a*) An unstable wave on the circle network, corresponding to equation (10) with $w = 0.8$, $\epsilon = 0$, $d = 1$. (*b*) The phase space configuration of a snapshot of the unstable wave in (*a*). (*c*) The corresponding x_i value on each node in (*b*). The plots (*d*), (*e*), (*f*) and (*g*), (*h*), (*i*) correspond to two other unstable waves on the same circle network.

In this section, possible solutions of the model equation (4) are classified or discussed briefly. Among the stable solutions, we identified the regular and the special waves. Furthermore, through extensive numerical experiments we found that in the region where nontrivial asymptotic solutions exist, the basin of attraction for regular waves or static solutions covers a large portion of the phase space. In other words, these types of solutions most likely appear when starting from an initial condition chosen randomly, which greatly facilitates exploration of the phase space orbit structure.

3.2. The general presence of regular nonlinear waves

The regular wave survives perturbation and continues to exist even when ϵ grows as large as ω or d, as shown in figure 4. In circle networks, regular nonlinear waves are the most commonly observed, which is attributed to the rotational symmetry of the system and quite independent of the local dynamics. We will perform a perturbation analysis of a generalized equation to
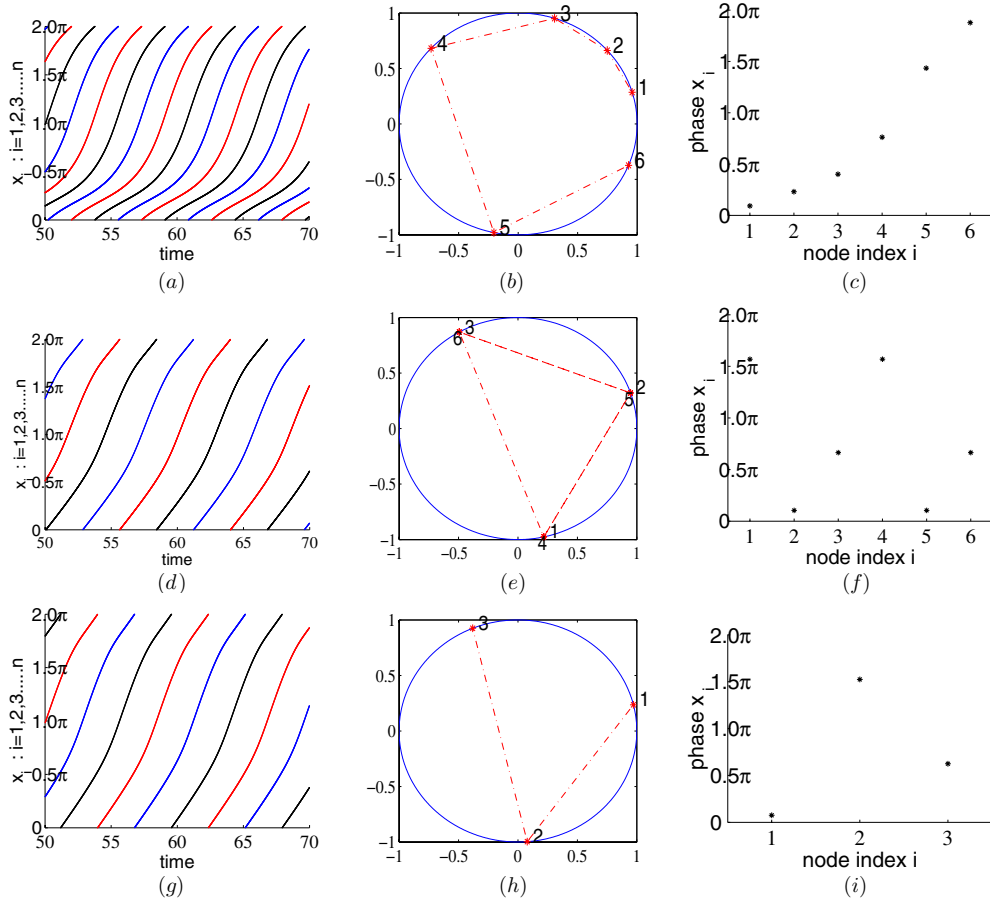
Figure 4. Regular nonlinear waves on the circle network with $w = 0.8$, $\epsilon = 1$, $d = 1$. See equation (23). $\langle (a), (b), (c) \rangle$ A regular nonlinear wave with $k = 1$, $n = 6$. $\langle (d), (e), (f) \rangle$ A regular nonlinear wave with $k = 2$, $n = 6$. $\langle (g), (h), (i) \rangle$ A regular nonlinear wave with $k = 1$, $n = 3$.

derive the expression of the period and the analytical form of the regular solution to the lowest order, thus showing the general features of regular nonlinear waves.

Let us consider a generalized form of equation (4)

$$\dot{x}_i = \omega - \epsilon g(x_i) + h(x_{i+1} + x_{i-1} - 2x_i), \quad x_i \in \mathbb{R}, \tag{15}$$

where g, h are both smooth 2π-periodic functions with $h(0) = 0, h'(0) > 0, h''(0) = 0$, and $\int_0^{2\pi} g(x)\mathrm{d}x = 0$. Note that if $h(0) \neq 0$, then $h(0)$ can be incorporated into ω. Besides, it is assumed that $a_0 = 1/2\pi \int_0^{2\pi} g(x)\mathrm{d}x = 0$, otherwise, the transformation

$$g(x) \to g(x) - a_0, \omega \to \omega - \epsilon a_0$$

gives the right form.

The Poincaré–Lindstedt method [30] is a well-known perturbation approach for approximating periodic solutions of ordinary differential equations. An introduction to the technique and justification of its usage here are given in appendix B. Below, by applying the Poincaré–Lindstedt perturbation technique, we compute the period and the analytic expression

of the regular nonlinear wave to the lowest order of ϵ. Its stability is also discussed. For $\epsilon \ll 1$, we assume that the time and the state variable have the following form

$$\tau = \Omega t, \qquad \Omega = \omega_0 + \epsilon\omega_1 + \epsilon^2\omega_2 + \cdots, \qquad x_i = x_{i,0} + \epsilon x_{i,1} + \epsilon^2 x_{i,2} + \cdots. \quad (16)$$

Then $x_i(\tau)$ is 2π-periodic and the period for $x_i(t)$ is $2\pi/\Omega$. After substituting equation (16) into equation (15), a comparison of different orders of ϵ leads to the set of equations that successively determines $x_{i,0}, x_{i,1}, x_{i,2}, \ldots$.

With the definition $\eta_i = x_{i+1,0} - x_{i,0}$, the zeroth order equation becomes

$$\omega_0 \frac{d\eta_i}{d\tau} = h(\eta_{i+1} - \eta_i) - h(\eta_i - \eta_{i-1}).$$

In this case, the regular nonlinear waves assume $\eta_i = -2k\pi/n$, $k = 0, 1, 2, 3, \ldots, n-1$. Then $\omega_0 = \omega$ since $\Omega = \omega$ when $\epsilon = 0$ and

$$x_{i,0} = \tau - \frac{2(i-1)k\pi}{n}.$$

The first order equation, upon substitution of the Fourier expansion for $g(\tau - \frac{2(i-1)k\pi}{n})$, then gives

$$\omega_1 + \omega\frac{dx_{i,1}}{d\tau} = \sum_{m=1}^{\infty}\left(a_m\sin\left(m\left(\tau - \frac{2(i-1)k\pi}{n}\right)\right) + b_m\cos\left(m\left(\tau - \frac{2(i-1)k\pi}{n}\right)\right)\right)$$
$$+ h'(0)(x_{i+1,1} + x_{i-1,1} - 2x_{i,1}), \quad (17)$$

where a_m, b_m are the Fourier coefficients for $g(x)$. Let $v_0 = \sum_{i=1}^{n} x_{i,1}$ and a summation of equation (17) over i results in $n\omega_1 + \omega\frac{dv_0}{d\tau} = 0$. To avoid secular terms, $\omega_1 = 0$ is taken, thus obtaining the periodicity condition

$$\omega\frac{dx_{i,1}}{d\tau} = \sum_{m=1}^{\infty}\left(a_m\sin\left(m\left(\tau - \frac{2(i-1)k\pi}{n}\right)\right) + b_m\cos\left(m\left(\tau - \frac{2(i-1)k\pi}{n}\right)\right)\right)$$
$$+ h'(0)(x_{i+1,1} + x_{i-1,1} - 2x_{i,1}). \quad (18)$$

Note that equation (18) is a linear differential equation with the driving term being a superposition of trigonometric functions. Hence, the response is a superposition of solutions for the component-wise equations, which can be solved based on equations (C.4) and (C.5) in appendix C and give

$$x_{i,1} = \sum_{m=1}^{\infty}\left((a_m A_m - b_m B_m)\sin\left(m\left(\tau - \frac{(i-1)2k\pi}{n}\right)\right)\right.$$
$$\left. + (a_m B_m + b_m A_m)\cos\left(m\left(\tau - \frac{(i-1)2k\pi}{n}\right)\right)\right),$$

where

$$A_m = \frac{4h'(0)\sin^2(k\pi/n)}{m^2\omega^2 + (4h'(0)\sin^2(mk\pi/n))^2}, \qquad B_m = -\frac{m\omega}{m^2\omega^2 + (4h'(0)\sin^2(mk\pi/n))^2}.$$

The second order equation with the substitution of $x_{i,0}$, $x_{i,1}$ and the assumption that $h''(0) = 0$ (so complicated nonlinear terms disappear) becomes

$$\omega_2 + \omega\frac{dx_{i,2}}{d\tau} = h'(0)(x_{i+1,2} + x_{i-1,2} - 2x_{i,2}) + \sum_{m=1}^{\infty}\left(a_m m\cos\left(m\left(\tau - \frac{2(i-1)k\pi}{n}\right)\right)\right.$$
$$\left. - b_m m\sin\left(m\left(\tau - \frac{2(i-1)k\pi}{n}\right)\right)\right)$$
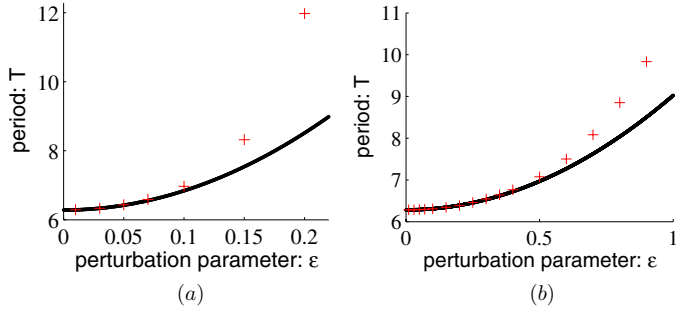
Figure 5. The dependence of $T(\epsilon)$ on ϵ of regular nonlinear waves. Simulation results are plotted as plus(+), while the analytical prediction is plotted as solid line. (*a*) Results from the system described by $\dot{x}_i = 1 - \epsilon(\sin(x_i) + 2\cos(2x_i) + 3\sin(3x_i) + 4\cos(4x_i)) + \sin(x_{i+1} + x_{i-1} - 2x_i)$, with $n = 10$, $k = 1$. The analytical prediction is $T = 54.9444\epsilon^2 + 6.2832$ according to equation (22). (*b*) Results from the system described by equation (4) with $n = 10$, $w = 1$, $d = 1$, $k = 1$. The analytical prediction is $T = 2.7415\epsilon^2 + 6.2831 + O(\epsilon^3)$, based on equation (24).

$$
\times \sum_{m=1}^{\infty} \left((a_m A_m - b_m B_m) \sin\left(m\left(\tau - \frac{(i-1)2k\pi}{n} \right) \right) \right.
$$
$$
\left. + (a_m B_m + b_m A_m) \cos\left(m\left(\tau - \frac{(i-1)2k\pi}{n} \right) \right) \right). \tag{19}
$$

Let $v_1 = \sum_{i=1}^{n} x_{i,2}$, a summation over i and integration from 0 to 2π of the above equation results in $2\pi n \omega_2 + \int_0^{2\pi} \omega \frac{dv_1}{d\tau} = \sum_{m=1}^{\infty} (mn\pi(a_m^2 B_m + b_m^2 B_m))$. To avoid secular terms, we take

$$
\omega_2 = \frac{\sum_{m=1}^{\infty} m(a_m^2 B_m + b_m^2 B_m)}{2}.
$$

Finally, we obtain a solution that is stable [31]

$$
x_i = \tau - \frac{2(i-1)k\pi}{n} + \epsilon \sum_{m=1}^{\infty} \left((a_m A_m - b_m B_m) \sin\left(m\left(\tau - \frac{(i-1)2k\pi}{n} \right) \right) \right.
$$
$$
\left. + (a_m B_m + b_m A_m) \cos\left(m\left(\tau - \frac{(i-1)2k\pi}{n} \right) \right) \right) + O(\epsilon^2), \tag{20}
$$

with

$$
\Omega = \omega + \frac{\sum_{m=1}^{\infty} m(a_m^2 B_m + b_m^2 B_m)}{2} \epsilon^2 + O(\epsilon^3), \tag{21}
$$

$$
T = \frac{2\pi}{\omega} - \frac{\sum_{m=1}^{\infty} m\pi(a_m^2 B_m + b_m^2 B_m)}{\omega^2} \epsilon^2 + O(\epsilon^3). \tag{22}
$$

The above perturbation analysis validates our vision that, in the context of circle networks, regular nonlinear waves exist stably as long as equation (15) is satisfied. Regular nonlinear waves for different local dynamics on circle networks are invariably observed in numerical simulation. In figure 5(*a*), we gave an example where the period $T(\epsilon)$ versus ϵ is plotted. When $\epsilon < 0.1$, the analytical results fit quite well with the simulation. However, when $\epsilon > 0.1$ the analytical results start to diverge, with higher order terms coming into play.

Based on the above analysis and the resulting equations (20)–(22), we have the following perturbation solution for equation (4) which is a special case of equation (15)

$$x_i = \tau - \frac{(i-1)2k\pi}{n} + \epsilon \left(B \cos\left(\tau - \frac{(i-1)2k\pi}{n}\right) + A \sin\left(\tau - \frac{(i-1)2k\pi}{n}\right)\right) + O(\epsilon^2),$$

(23)

$$\Omega = \omega - \frac{B}{2}\epsilon^2 + O(\epsilon^3),$$

$$T = \frac{2\pi}{w} + \frac{B\pi}{w^2}\epsilon^2 + O(\epsilon^3),$$

(24)

where

$$\tau = \Omega t, \qquad A = -\frac{4d\sin^2(k\pi/n)}{w^2 + 16d^2\sin^4(k\pi/n)}, \qquad B = \frac{w}{w^2 + 16d^2\sin^4(k\pi/n)}.$$

In figures 4(a) and (d), it is easy to see that the nonlinear wave has the property of equal-time-separation, while the phase space separations between the x_i are different, as illustrated in figures 4(c) and (f). In the case of equation (23), the phase separation $\Delta t = kT/n$ for $k \neq 0$. When $k = 0$, all the nodes fully synchronize and there is no phase difference.

Thus, the perturbation analysis gives the nonlinear wave solution which is stable when $d > 0$. On the circle network, the variable k in equation (23) indicates the wavenumber for the nonlinear wave. The corresponding wavelength λ is n/k. Regular nonlinear waves with different wavenumbers are shown in figure 4. In the phase space, wavenumbers can be easily calculated by counting the number of circuits for which the consecutive node 1, 2, ..., n winds around the circle. Thus, the wavenumber is 1 for figures 4(b) and 2 for figures 4(e). From equation (24), it is easy to see that both the period and the frequency depend on ϵ quadratically to the lowest order. The configuration is recurrent on the circle network in a regular time interval T. The dependence of T on ϵ is computed numerically and agrees quite well with the analytical approximation equation (24) for $\epsilon < 0.5$, as shown in figures 5(b). For bigger ϵ, the actual period is larger than the analytical result, which indicates a non-negligible role of higher order terms. It is expected that at some finite value of ϵ depending on the coupling d and the wavenumber k, the regular nonlinear wave ceases to exist and the stable solution is a fixed point which corresponds to a uniform and stationary phase configuration.

The regular nonlinear waves in the current model are closely related to those of the two-dimensional models, such as the Bär–Eiswirth model (1). Regular nonlinear waves with wavenumbers $k = 1, 2$ for the Bär–Eiswirth model are depicted in figure 6. In figure 6(d), the node i and node $(i + 6)(\mathrm{mod}\,12)$ synchronize, resulting from the periodicity of the circle network. The nonlinear wave in figure 6(d) is actually constructed from the one in figure 6(a). In simulations, regular nonlinear waves for $n < 6$ have not been found. By comparing figures 4 and 6, we see that regular nonlinear waves are simple yet universal for circle networks, which are significant for the analysis of pattern formation in complex networks.

A key concept from the Frenkel–Kontorova model is the phase gradient across the system, i.e., $\Delta x_i = x_i - x_{i-1}$. The analysis in this work mainly addresses the case of a constant phase gradient, i.e., regular solutions for $\epsilon \to 0$. Given an arbitrary initial condition, regular nonlinear waves are more likely to be selected according to our simulation. This can be partly explained in terms of the soliton, which is a fundamental solution for the Frenkel–Kontorova model. More complicated wave patterns can be constructed with multiple solitons. Presumably, due to the repulsive interaction between the solitons, the phase gradient tends to become uniform when the lattice pinning effect [20] vanishes, i.e., $\epsilon \to 0$, thus resulting in regular nonlinear waves.
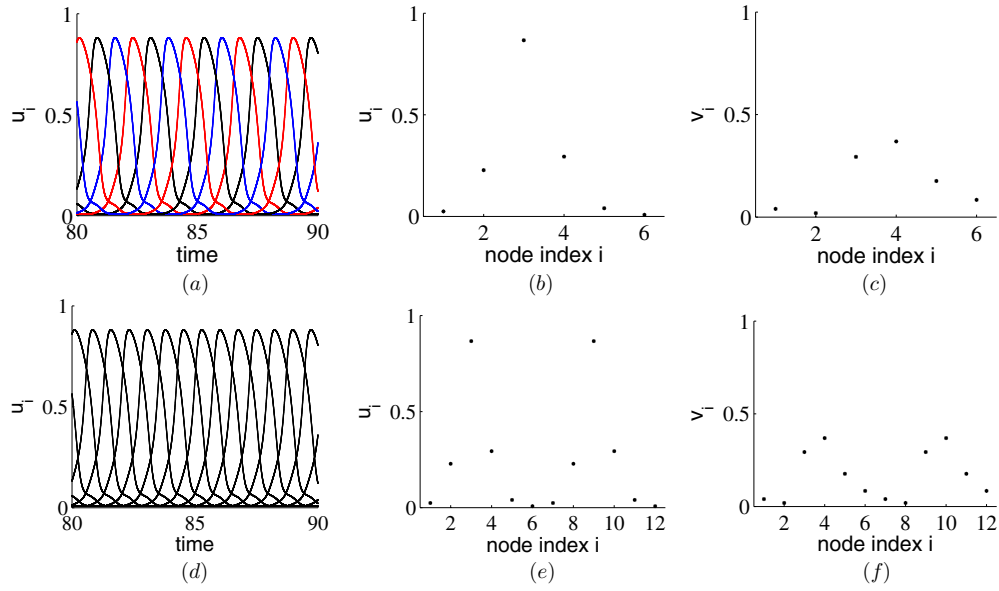
Figure 6. Regular nonlinear waves on the circle network for the revised Bär–Eiswirth model, with $\epsilon = 0.04$, $b = 0.15$, $a = 0.84$, $d = 1$, see equation (1). In (*a*), (*b*), (*c*), a regular nonlinear wave with $k = 1$, $n = 6$, where (*a*) depicts the dynamics of $u_i(t)$, (*b*) shows a snapshot of u_i and (*c*) shows a snapshot of v_i. In (*d*), (*e*), (*f*), a regular nonlinear wave with $k = 2$, $n = 12$.

3.3. Stable solutions with $\beta \neq 0$

Stable solutions for $\beta \neq 0$ are also observed and only appear in the discrete case, as illustrated in figure 7. These special type of solutions, if viewed as nonlinear waves, have nearly all nodes synchronized in pairs, leaving one (when n is odd) or two (when n is even) nodes moving alone.

In the general solution (13), when n is odd, we may take $k = (n + 1)/2$ in the constraint equation (12) such that $\eta_1 = \beta$. In this case,

$$x_i = x_{n+1-i}, \quad i \in \left\{1, 2, 3, \ldots, \frac{n-1}{2}\right\}. \tag{25}$$

When n is even, we may take $k = n/2$ in equation (12) so that $\eta_1 = \beta/2$. In this case,

$$x_i = x_{n+2-i}, \quad i \in \left\{2, 3, \ldots, \frac{n}{2}\right\}. \tag{26}$$

The discussion above is also applicable to the circumstance with $\epsilon > 0$. figure 7 demonstrates two typical special nonlinear waves with $\epsilon = 0.05$. In figure 7(*b*), we see that the node pairs $(1, 7)$, $(2, 6)$, $(3, 5)$ synchronize while node 4 is left alone, in accordance with equation (25). In figure 7(*e*), the node pairs $(2, 10)$, $(3, 9)$, $(4, 8)$, $(5, 7)$ synchronize while nodes 1 and 6 are left alone, corresponding to equation (26). A comparison of configurations has been made between special nonlinear waves computed numerically with $\epsilon > 0$ (red stars) and their counterparts with $\epsilon = 0$ by equation (13) (blue stars), as illustrated in figures 7(*b*) and (*e*). It seems that the analytical solution with $\epsilon = 0$ is a good approximation for small ϵ.

When $\epsilon = 0$, we have

$$T = \frac{2\pi}{w + d\sin(\beta)}, \tag{27}$$
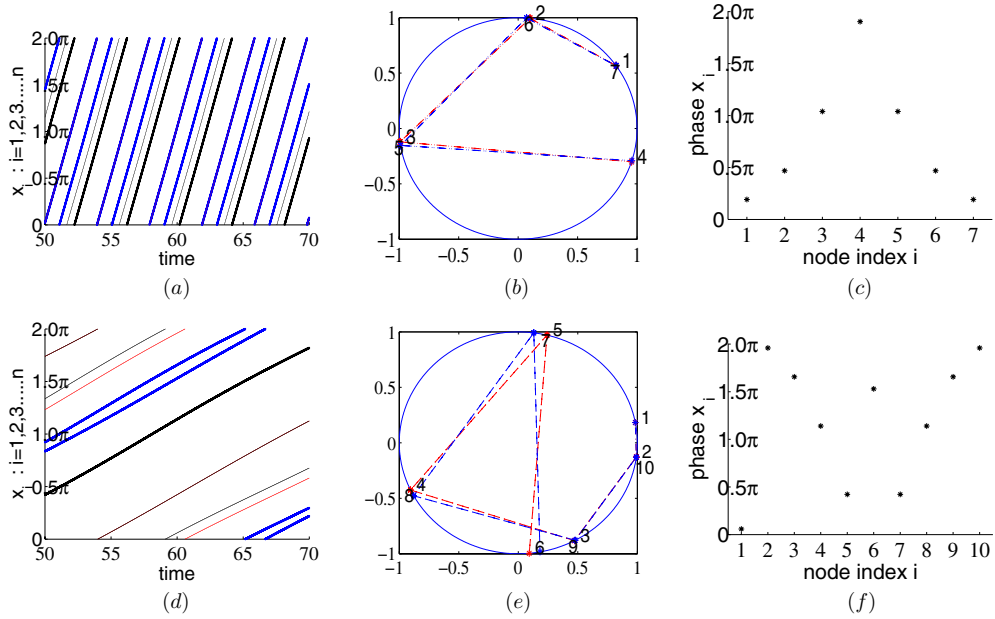
Figure 7. Typical stable special nonlinear waves. (*a*), (*b*), (*c*) plot a special nonlinear wave on the circle network, with $n = 7$, $w = 0.8$, $\epsilon = 0.05$, $d = 1$, $p = 1$ for equations (25) and (27). (*d*), (*e*), (*f*) plot a special nonlinear wave on the circle network, with $n = 10$, $w = 0.8$, $\epsilon = 0.05$, $d = 1$, $p = -1$ for equations (26) and (27). The blue stars in (*b*) and (*e*) indicate the corresponding analytical solution with $\epsilon = 0$ in equation (13).

where $\beta = 2p\pi/n$. In all special nonlinear waves, the ones with smaller $|p|$ are more likely to be observed. Compared with the period of the counterpart regular nonlinear wave with the same ω, ϵ, d, negative p lead to longer periods and positive p to shorter ones. To show how well equation (27) approximates the period of the special nonlinear wave with $\epsilon \neq 0$, a numerical result is displayed in figure 8. The analytical expression gives a good prediction when ϵ is relatively small. The relative error is less than 2% when $\epsilon \leqslant 0.2$. When ϵ increases over a critical value ϵ_c, the special nonlinear wave becomes unstable. In each case displayed in figure 8, the result with the largest ϵ (i.e., equal to ϵ_c) corresponds to the special nonlinear wave that is at the brim of being unstable. As the simulation shows, ϵ_c depends on d, w, n, p.

In figures 8(*b*) and (*d*) for $p = -1$, the dependence of the period T shows a non-monotonic behavior on the size of perturbation: it increases when ϵ is small but decreases after passing a maximum, which is very different from that of a regular solution. The detailed dependence of $T(\epsilon)$ on ϵ and its physical implication remain to be explored.

Special nonlinear waves seem to be universally present in circle networks since they are easily observed in the general one-dimensional model (3) with different local dynamics. In figure 5(*b*), an example is presented where special nonlinear waves are observed for $\epsilon \leqslant 0.22$. The special solution corresponds to a finite curvature in the phase field, i.e., a variable phase gradient in the Frenkel–Kontorova model [20].

In the above study, we find that the regular and the special waves are the most easily observed stable solutions of our system. Although it is difficult to analytically identify the stable and unstable parameter range, numerical computation gives a hint as to what they look like as shown in figure 9 for a typical regular and special wave solution. We can see that either in the excitable region, i.e. $\omega < \epsilon$, or the non-excitable region, both regular (figure 9(*a*)) and
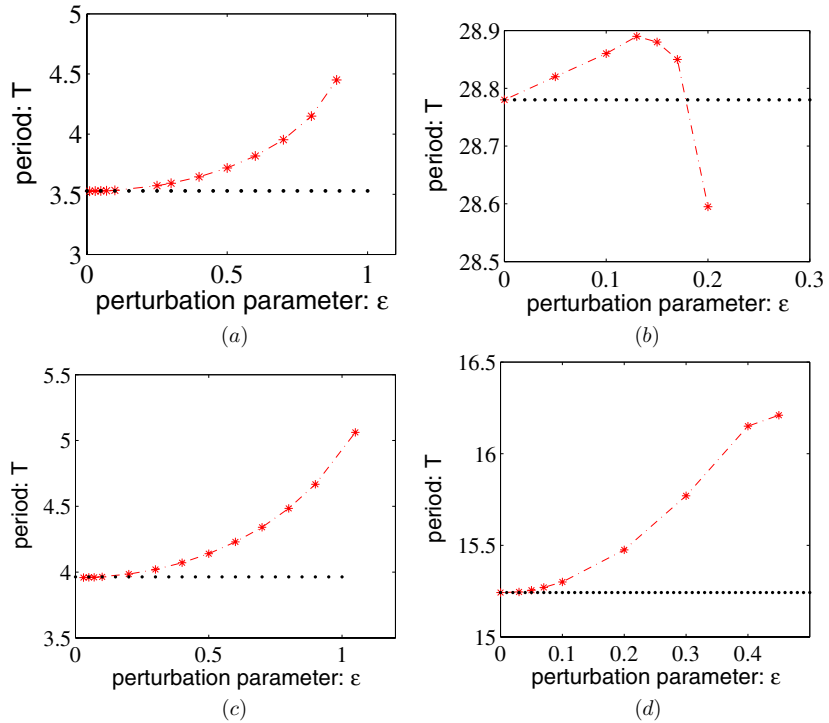
Figure 8. The dependence of the period on ϵ for different stable special nonlinear waves. Simulation results are plotted as red stars (with a dashed line), along with the analytic result for $\epsilon = 0$ serving as the baseline, which are plotted as black dots. (*a*) The parameter values are $n = 7$, $w = 0.8$, $d = 1$, $p = 1$ in equations (25) and (27). (*b*) The same as (*a*) except that $p = -1$. (*c*) $n = 10$, $w = 0.8$, $d = 1$, $p = 1$ in equations (26) and (27). (*d*) The same as (*c*) but $p = -1$.
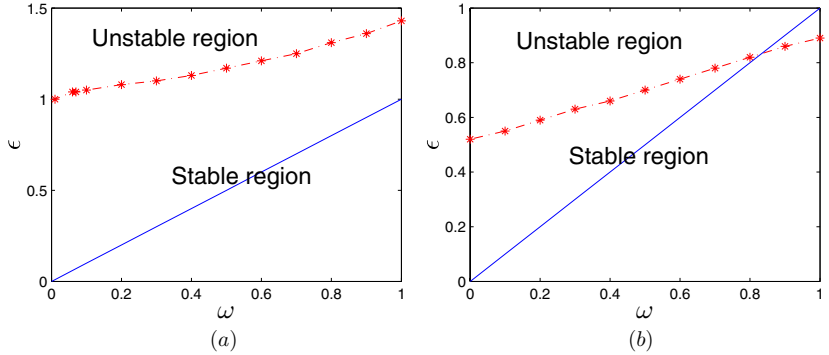
Figure 9. Stability phase diagram for specific solutions. Here, d is fixed to be 1 and we change ω, ϵ to study the stability of one specific solution. The separatrix between the stable region and unstable region is indicated by the red dotted line with stars. The solid blue line is $\omega = \epsilon$, which is the boundary of the excitable and non-excitable local dynamics. (*a*) Phase diagram for the solution shown in figure 4(*a*). (*b*) Phase diagram for the solution shown in figure 7(*a*).

special solutions (figure 9(*b*)) emerge. However, the regular wave possesses a larger stability region and is stable whenever $\epsilon < 1$. The boundaries that separate the stable and the unstable region seem monotonic in both cases: larger ω or smaller ϵ lead to more stable solutions,
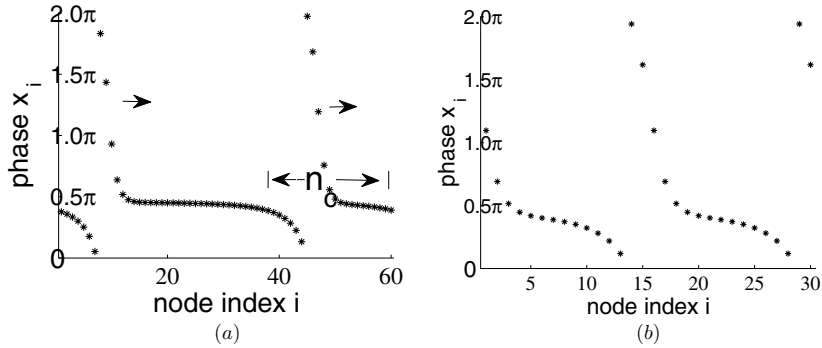
Figure 10. (a) Two independent circulating pulses on a circle network with $n = 60$, $w = 0.99$, $\epsilon = 1$, $d = 1$. The direction of movement is indicated by the arrow. n_c is the number of nodes covered by one pulse. (b) A regular nonlinear wave with $k = 2$, $n = 30$, $w = 0.99$, $\epsilon = 1$, $d = 1$.

which is understandable since this range of parameters corresponds to more easily excitable local dynamics. One interesting observation is that certain special nonlinear waves become unstable even for $\epsilon < \omega$ when ω is large as indicated by the intersection of the solid and the dashed lines in figure 9(b).

4. Circulating pulse and regular nonlinear wave

Our model is closely related to the excitable media on a circle. In previous studies, a circulating pulse was rendered unstable and changed to a steady solution upon decreasing the circumference of the ring [15, 16]. In our discrete model, pulses would first change to regular nonlinear waves with decreasing n. The difference between circulating pulses and regular nonlinear waves is explained in figure 10. In figure 10(a), the two pulses do not constitute a regular nonlinear wave, since the distance between them may be adjusted freely as long as it is larger than the critical number n_c, where n_c is the number of nodes spanned by a single pulse, thus contradicting the uniqueness of the regular nonlinear wave with $k = 2$. Note that for the circulating pulses in figure 10(b) the node indices corresponding to peaks are $i_{peak1} = 8$, $i_{peak2} = 45$ and thus $i_{peak2} - i_{peak1} \neq n/2 = 30$, while $i_{peak2} - i_{peak1} = n/2$ for a regular nonlinear wave, e.g. the one in figure 10(b). When n decreases to 30, the two pulses strongly interact with each other and a regular nonlinear wave with $k = 2$ emerges. So a circulating pulse can be viewed as a local structure, which spreads over n_c nodes in the circle network, as indicated in figure 10(a). Two pulses will change to a regular nonlinear wave if they overlap. This phenomenon is characteristic of the discreteness of our model on a circle network.

  The circulating pulse is similar to the soliton solution of the Frenkel–Kontorova model. The stability of the circulating pulse is due to the excitable property of individual nodes, while the stability of the soliton is also well explained in the Frenkel–Kontorova model in terms of the lattice pinning effect [20], i.e., the potential well created by the discreteness of lattice. Our model describes the lattice pinning effect and the excitability property in an equivalent and unified way.

  The recovery time and the pulse duration are two important physical observables in the evolution of excitable node dynamics and have been well characterized in the literature [16]. In our case, the recovery time t_r is the time spent in overcoming the barrier between two fixed points defined by the local dynamics (i.e., $x_{fix1} = \arcsin(w)$, $x_{fix2} = \pi - \arcsin(w)$):
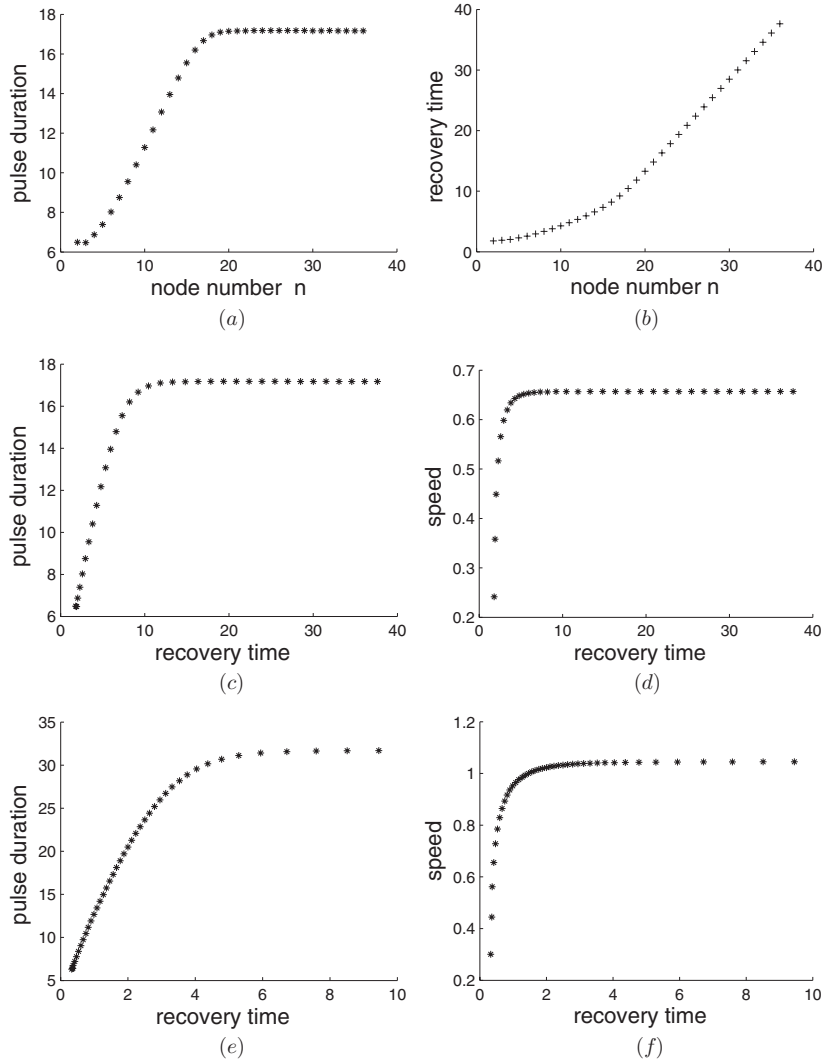
Figure 11. Useful characteristics of the circulating pulse in a circle network. $d = 1$, $\epsilon = 1$ in all plots. (*a*) The pulse duration a as a function of the total node number n, with $\omega = 0.8$. (*b*) The recovery time $t_r(n)$, with $\omega = 0.8$. (*c*) The restitution curve $a(t_r)$ with $\omega = 0.8$. (*d*) The dispersion curve $c(t_r)$ with $\omega = 0.8$. (*e*) The restitution curve $a(t_r)$ with $\omega = 0.99$. (*f*) The dispersion curve $c(t_r)$ with $\omega = 0.99$.

$t_r = t_2 - t_1$, where $x(t_1) = x_{\text{fix1}}$, $x(t_2) = x_{\text{fix2}}$. The pulse duration $a = T - t_r$ is the time spent in the long excursion away from the fixed points. Due to the rotational symmetry of our model, t_r and a are independent of node position in the circle network, but strongly dependent on the circumference n. A careful simulation is undertaken to determine the curves $t_r(n)$, $a(n)$, $a(t_r)$, $c(t_r)$, shown in figure 11, where c is the speed of the circulating wave defined by $c = n/(t_r(n) + a(n))$. The curve $a(t_r)$ is termed the *restitution curve* and $c(t_r)$ the *dispersion curve*. These curves are important in that they help us understand relevant and universal properties for circulating pulses in a circle network [16].

In figures 11(*a*) and (*b*), there is a turning point in $a(n)$ and $t_r(n)$ around $n = 18$, which signifies a transition from a regular nonlinear wave to a circulating pulse. The saturation in $a(n)$

and the constant slope for $t_r(n)$ when $n > 18$ is characteristic of a circulating pulse, simply because the pulse does not spread over all nodes and moves at a constant speed along the circle network for n large enough. Thus the critical number n_c of nodes covered by a pulse can be defined as n at the transition point. Geometrically, on the phase circle, an increasing number of nodes are moving at the recovery stage with a decreased speed and have thus increased the recovery time. The density of the nodes on the excursion contour remains constant for large n, leading to a constant duration time. The *restitution curve* $a(t_r)$ and the *dispersion curve* $c(t_r)$ are plotted in figure 11 with different ω which look qualitatively similar. The difference originates from disparate distances between fixed points of the local dynamics. The saturation of $a(t_r)$ and $c(t_r)$ is also associated with the transition from a regular nonlinear wave to a pulse. Similar saturation behavior was observed in a one-dimensional ring of excitable media with a very sophisticated description of motion dynamics [16]. The physical observables $t_r(n)$, $a(n)$, $a(t_r)$, $c(t_r)$ used here are universal quantities for characterizing circulating pulses in a circle network.

5. Summary

Previous works [14] suggest that the dynamics of coupled excitable nodes on a complex network may have a very simple yet universal structure, which includes self-sustained oscillation on the circle sub-network and attached branches driven by the center oscillation. This paper focuses on a discussion of possible solutions for a new type of equation, which is simple enough for analytic computation yet captures the essence of nonlinear wave generation and propagation on networks with excitable nodes. This new model can be viewed as a most direct extension of the Kuramoto model to treat the excitable dynamics, the understanding of which will help us to study the possible behavior of other models with excitable dynamics on complex networks due to its generality.

In this paper, we carried out a quite thorough study of the new model on circle networks, and revealed certain common features of regular solutions, which is quite independent of the local dynamics and the attached branches being driven, and closely related to the Laplacian coupling of neighboring nodes. Although there are numerous solutions for this system, in terms of stability and the basin of attraction, regular nonlinear waves and, in the case of large number of nodes, circulating pulses are the most important ones, which is confirmed by simulation. The period T for regular nonlinear waves is computed analytically, and agrees well with the numerical result up to $\epsilon \sim 0.5\omega$. An analytic form of the regular nonlinear wave is also obtained to first order. A new type of solution, the special nonlinear wave, is also studied and compared to the regular solution. It is stable in a certain parameter regime but only exists for the discrete dynamics. The properties of circulating pulses on circle networks with excitable nodes are discussed in detail and their relevance to the regular solution is also studied.

Our model is closely related to the Frenkel–Kontorova model. While the classical Frenkel–Kontorova model describes the Newtonian dynamics of a chain of classical particles, here we use the over-damped version with a special form of coupling to study pattern formation on complex networks. The simplicity of this model and previous understanding of the Frenkel–Kontorova model hopefully give physical insights while still keeping the analytic understanding within reach.

Much more work needs to be done. For example, the existence condition and the basin of attraction for each regular solution should be more precisely characterized. Further, we may employ the current model to study the interaction of the circle sub-network and the attached branches in a network of general topology, or the interaction of real complex networks. It

would be interesting to compare wave propagation on the same network but with different excitable dynamics.

Appendix A. Stability of solutions

Let us consider the stability of solutions for equation (8). We write the perturbation solution in this form $\eta_i^{(p)} = \eta_i + \epsilon_i$, in which η_i is the stationary solution for equation (8) and satisfies equation (11). Ignoring higher order terms of ϵ, a substitution of $\eta_i^{(p)}$ into equation (8) gives

$$\frac{d\epsilon_i}{dt} = \alpha(\epsilon_{i+1} + \epsilon_{i-1} - 2\epsilon_i), \tag{A.1}$$

where $\alpha = d\cos(\beta)$. Suppose $\alpha > 0$, then

$$\frac{d\vec{\epsilon}}{d\tau} = -\alpha Q\vec{\epsilon} = A\vec{\epsilon}.$$

So Q can be viewed as a Laplacian matrix of the circle network. It turns out that Q is a positive semi-definite matrix, with eigenvalues $0 = \lambda'_0 \leqslant \lambda'_1 \leqslant \ldots \leqslant \lambda'_{n-1}$. So the eigenvalues λ_i for $A = -\alpha Q$ are all non-positive if $\alpha > 0$.

More specifically, suppose

$$\epsilon_i = a e^{j\frac{2mi\pi}{n}} e^{\lambda_m \tau}, \quad m = 0, 1, \ldots n - 1,$$

where $j = \sqrt{-1}$. Then $\lambda_m = -4\alpha \sin^2(m\pi/n)$, which are the eigenvalues of this system. All the eigenvectors for $m > 0$ correspond to the stable direction and the one for the eigenvalue $\lambda_0 = 0$ corresponds to the rotation of the system as a whole. Therefore, up to a rotation, the solution is stable and the larger α is, the more stable the solution will be. From the discussion above, we conclude that $\alpha > 0$ gives stable solutions while $\alpha = 0$ neutrally stable solutions and $\alpha < 0$ unstable solutions.

However, the following situation

$$\exists m, \eta_{m+1} - \eta_m = \beta \text{ and } \eta_m - \eta_{m-1} = \pi - \beta$$

for the stationary solution of equation (8) is more difficult to analyze. This situation may possibly, though not necessarily, bring instability to the system. Numerical simulation results show that that the system would be unstable under this condition in most cases except a few.

Appendix B. The Poincaré–Lindstedt method

In seeking a periodic solution, the regular perturbation technique usually fails because the period of the new solution is slightly different from that of the unperturbed one which the perturbation expansion starts from. The mismatch of the two periods usually results in secular terms which grow without bound. The Poincaré–Lindstedt method overcomes this shortcoming by allowing stretching or compressing of the time coordinate, thus matching the two periods. To implement this method, we need to make sure that the periodic solution exists and the expansion converges at least for the small perturbation. Below, we briefly review the theorem on the existence of periodic solutions and then verify that our general model satisfies the existence conditions.

B.1. The existence of periodic solutions

Consider in $\mathbb{R}^n$ the equation

$$\dot{x}_i = f_i(\vec{x}) + \epsilon g_i(\vec{x}), \tag{B.1}$$

where ϵ is a small parameter, $i \in \{1, 2, \ldots, n\}$, $\vec{x} = (x_1, x_2, \ldots, x_n)$, $f_i(\vec{x}) = f_i(x_1, x_2, \ldots, x_n)$ and $g_i(\vec{x}) = g_i(x_1, x_2, \ldots, x_n)$. We are seeking the periodic solutions of the equation. For the unperturbed equation

$$\dot{y}_i = f_i(\vec{y}),$$

it is assumed that a T_0-periodic solution

$$y_i = G_i(t; \varphi_1, \varphi_2, \ldots, \varphi_n) \tag{B.2}$$

exists with the φ_i being integral constants. To get a periodic solution for equation (B.1), it is convenient to make a coordinate transformation

$$\Omega t = \tau, \Omega^{-1} = \omega^{-1} + \epsilon \phi_0(\epsilon),$$

with Ω being the frequency of the new solution and $\omega = 2\pi/T_0$. This transformation allows us to directly approximate the new period. After this transformation, the new solution sought is 2π-periodic in τ. A perturbation expansion of the solution for equation (B.1) could be written as

$$x_i = M_i(\tau; \phi_0, \phi_1, \phi_2, \ldots, \phi_n, \epsilon). \tag{B.3}$$

Denote

$$H_i(\vec{\phi}, \epsilon) = M_i(2\pi; \phi_0, \phi_1, \phi_2, \ldots, \phi_n, \epsilon) - M_i(0; \phi_0, \phi_1, \phi_2, \ldots, \phi_n, \epsilon),$$

where $\vec{\phi} = (\phi_0, \phi_1, \ldots, \phi_n)$. The periodicity condition requires

$$H_i(\vec{\phi}, \epsilon) = 0, \tag{B.4}$$

which determines n parameters from the n periodicity conditions equation (B.4) in the neighborhood of $\epsilon = 0$. The extra parameter corresponds to the time translational symmetry of the autonomous equations. equation (B.4) is equivalent to

$$\text{rank}\left(\frac{\partial \vec{H}}{\partial \vec{\phi}}\right) = n, \tag{B.5}$$

where $\vec{H} = (H_1, H_2, \ldots, H_n)^T$ and $\frac{\partial \vec{H}}{\partial \vec{\phi}}$ is the Jacobian matrix of $\vec{H}$. This is also called the uniqueness condition since it determines uniquely the new periodic solution up to a time translation.

Below we state theorems relevant to the Poincaré–Lindstedt method. See [31] (chapters 9 and 10) for more details.

The Poincaré expansion theorem addresses the problem of the convergence of the usual perturbation solution of differential equations within certain time scale. And it roughly states that if $f_i(\vec{x})$ and $g_i(\vec{x})$ of equation (B.1) can be expanded in a convergent power series with respect to $\vec{x}$, then regular perturbation series converge in the neighborhood of $\epsilon = 0$ and the original initial condition within a time-scale 1.

The uniqueness theorem of periodic solutions concludes that If the uniqueness condition equation (B.5) is satisfied for equation (B.1), along with the requirement of the Poincaré expansion theorem and the periodicity condition equation (B.4), then there exists a periodic solution which can be represented by a convergent power series in ϵ in the form of equation (B.3) for $0 \leqslant \epsilon < \epsilon_0$ for some positive ϵ_0.

B.2. Justification

Now we justify the application of the Poincaré–Lindstedt method to our generalized model equation (15), which apparently satisfies the condition of the Poincaré expansion theorem since $g(x)$, $h(x)$ are both smooth functions. Below, we check the uniqueness and periodicity conditions.

Under the coordinate transformation

$$\Omega t = \tau, \quad \Omega^{-1} = \omega^{-1} + \phi_0(\epsilon),$$

where $\phi_0(\epsilon) = O(\epsilon)$, equation (15) becomes

$$\frac{dx_i}{d\tau} = 1 + \omega\phi_0 - \left(\frac{\epsilon}{\omega} + \epsilon\phi_0\right)g + \left(\phi_0 + \frac{1}{\omega}\right)h. \tag{B.6}$$

For the unperturbed equation

$$\frac{dy_i}{d\tau} = 1 + \frac{1}{\omega}h(y_{i+1} + y_{i-1} - 2y_i),$$

the regular solution is

$$y_i(\tau) = \tau - \frac{2(i-1)k\pi}{n}.$$

We can express the regular solution for equation (B.6) as

$$x_i(\tau) = \tau - \frac{2(i-1)k\pi}{n} + \phi_i + \int_0^\tau \left(\omega\phi_0 - \left(\frac{\epsilon}{\omega} + \epsilon\phi_0\right)g(x_i(\theta))\right.$$
$$\left. + \left(\phi_0 + \frac{1}{\omega}\right)h(x_{i+1}(\theta) + x_{i-1}(\theta) - 2x_i(\theta))\right)d\theta, \tag{B.7}$$

where $\phi_i = O(\epsilon)$ is a constant parameter and $\phi_i|_{\epsilon=0} = 0$. In accordance with the Poincaré expansion theorem, we assume that

$$y_i = x_i + O(\epsilon), \tag{B.8}$$

then $x_{i+1}(\theta) + x_{i-1}(\theta) - 2x_i(\theta) \approx O(\epsilon)$, thus

$$h(x_{i+1} + x_{i-1} - 2x_i) = h(0) + h'(0)O(\epsilon) + o(\epsilon) = O(\epsilon).$$

Then

$$\int_0^\tau \left(\omega\phi_0 - \left(\frac{\epsilon}{\omega} + \epsilon\phi_0\right)g(x_i) + \left(\phi_0 + \frac{1}{\omega}\right)h(x_{i+1} + x_{i-1} - 2x_i)\right)d\theta = O(\epsilon),$$

which is consistent with equation (B.8). A substitution of y_i for x_i at the right side of equation (B.6) with the notation $z_i = y_i + \phi_i$ gives

$$x_i(\tau) = z_i + \int_0^\tau \left(\left(\omega\phi_0 - \frac{\epsilon}{\omega}g(z_i)\right) + \frac{h'(0)}{\omega}(z_{i+1} + z_{i-1} - 2z_i)\right)d\theta + o(\epsilon). \tag{B.9}$$

The periodicity condition is

$$x_i(2\pi) = x_i(0) + 2\pi,$$

which, with the notation

$$H_i = \int_0^{2\pi} \left(\left(\omega\phi_0 - \frac{\epsilon}{\omega}g(z_i)\right) + \frac{h'(0)}{\omega}(z_{i+1} + z_{i-1} - 2z_i)\right)d\theta + o(\epsilon)$$

is equivalent to

$$H_i(\phi_0, \phi_1, \ldots, \phi_n) = 0, \quad i \in \{1, 2, \ldots, n\}.$$

Below, we calculate the Jacobian matrix of $\vec{H}$ in the neighborhood of $\epsilon = 0$ and $\vec{\phi} = 0$, where $\vec{\phi} = (\phi_0, \phi_1, \ldots, \phi_n)$:

$$\frac{\partial H_i}{\partial \phi_0} = 2\pi\omega, \quad i \in \{1, 2, \ldots, n\},$$

$$\frac{\partial H_i}{\partial \phi_i} = \int_0^{2\pi} \left(-\frac{g'(z_i)}{\omega} - 2\frac{h'(0)}{\omega} \right) d\theta, \quad i \in \{1, 2, \ldots, n\}.$$

Note that g is a 2π-periodic function, thus

$$\int_0^{2\pi} \left(-\frac{g'(z_i(\theta))}{\omega} d\theta \right) = \int_{z_i(0)}^{z_i(0)+2\pi} \left(-\frac{g'(z_i(\theta))}{\omega} dz_i \right) = -\frac{g(z_i(0)+2\pi) - g(z_i(0))}{\omega} = 0.$$

Then

$$\frac{\partial H_i}{\partial \phi_i} = -2\frac{2\pi h'(0)}{\omega}, \quad i \in \{1, 2, \ldots, n\}.$$

Besides,

$$\frac{\partial H_i}{\partial \phi_m} = \frac{2\pi h'(0)}{\omega}(\delta(m - i - 1) + \delta(m - i + 1)),$$

where $m, i \in \{1, 2, \ldots, n\}$, $m \neq i$ and

$$\delta(s) = \begin{cases} 1, & s = 0 \\ 0, & s \neq 0. \end{cases}$$

Finally, we obtain the Jacobian matrix for $\vec{H}$

$$\frac{\partial \vec{H}}{\partial \vec{\phi}} = \frac{2\pi h'(0)}{\omega} \begin{bmatrix} a & -2 & 1 & & & & 1 \\ a & 1 & -2 & 1 & & & \\ a & & 1 & -2 & 1 & & \\ \vdots & & & \ddots & \ddots & \ddots & \\ a & & & & 1 & -2 & 1 \\ a & 1 & & & & 1 & -2 \end{bmatrix}, \tag{B.10}$$

where $a = \frac{\omega^2}{h'(0)}$. This is an $n \times (n + 1)$ matrix with n linearly independent column vectors, thus

$$\text{rank}\left(\frac{\partial \vec{H}}{\partial \vec{\phi}} \right) = n,$$

which is just what the uniqueness condition requires for the existence of periodic solutions. According to the theorem of existence of periodic solutions, periodic solutions exist in our general model and the Poincaré–Lindstedt method can be applied.

Appendix C. Response to spatiotemporally periodic driving force

On a circle network, with diffusive coupling and subject to a spatiotemporal periodic driving, the equation of motion has the form

$$\dot{f}_i = F(i, t) + d(f_{i-1} + f_{i+1} - 2f_i), \tag{C.1}$$

where $F(i, t) = F(i+n, t) = F(i, t+T)$ with n being the number of nodes and T the period of the driving. With some minor assumptions, a periodic solution to this equation would be stable if $d > 0$, because the linearized equation takes the form of equation (A.1). In the following, we are mainly interested in the type of equations that are relevant to the proof in section 3.2.

Firstly, consider

$$F(i, t) = a \exp\left(j\left(mt - \frac{(i-1)2km\pi}{n} \right) \right),$$

where j is the imaginary number unit. Suppose the solution takes the form

$$f_i(t) = A \exp(j(mt - m(i-1)2k\pi/n)), \tag{C.2}$$

and substituting it into equation (C.1) results in

$$A = \frac{a}{jm + 4d \sin^2\left(\frac{mk\pi}{n} \right)}.$$

With this basic solution, we can easily calculate solutions for other types of driving terms. Consider

$$F(i, t) = a \sin\left(mt - \frac{(i-1)m2k\pi}{n} \right). \tag{C.3}$$

An implementation of equation (C.2) leads to

$$
\begin{aligned}
f_i(t) = {} & \frac{4ad \sin^2(mk\pi/n)}{m^2 + (4d \sin^2(mk\pi/n))^2} \sin\left(mt - \frac{m(i-1)2k\pi}{n} \right) \\
& - \frac{am}{m^2 + (4d \sin^2(mk\pi/n))^2} \cos\left(mt - \frac{m(i-1)2k\pi}{n} \right).
\end{aligned}
\tag{C.4}
$$

The cosine driving

$$F(i, t) = a \cos\left(mt - \frac{(i-1)2mk\pi}{n} \right),$$

gives then

$$
\begin{aligned}
f_i(t) = {} & \frac{am}{m^2 + (4d \sin^2(mk\pi/n))^2} \sin\left(mt - \frac{m(i-1)2k\pi}{n} \right) \\
& + \frac{4ad \sin^2(mk\pi/n)}{m^2 + (4d \sin^2(mk\pi/n))^2} \cos\left(mt - \frac{m(i-1)2k\pi}{n} \right).
\end{aligned}
\tag{C.5}
$$

All the solutions obtained above are stable nonlinear waves on the circle network, driven by a spatiotemporally periodic force.

References

[1] Peskin C 1975 *Mathematical Aspects of Heart Physiology* (New York: Courant Institute of Mathematical Sciences)
[2] Michaels D, Matyas E and Jalife J 1987 *Circ. Res.* **61** 704
[3] Ghosh A, Chance B and Pye E 1971 *Arch. Biochem. Biophys.* **145** 319
[4] Aldridge J *et al* 1976 *Nature* **259** 670
[5] Buck J 1988 *Q. Rev. Biol.* **63** 265
[6] Buck J and Buck E 1976 *Sci. Am.* **234** 74
[7] Jiang Z and McCall M 1993 *J. Opt. Soc. Am.* B **10** 155
[8] Kourtchatov S, Likhanskii V, Napartovich A, Arecchi F and Lapucci A 1995 *Phys. Rev.* A **52** 4089
[9] York R and Compton R 1991 *IEEE Trans. Microw. Theory Tech.* **39** 1000
[10] Wiesenfeld K, Colet P and Strogatz S 1996 *Phys. Rev. Lett.* **76** 404
[11] Acebrón J, Bonilla L, Vicente C, Ritort F and Spigler R 2005 *Rev. Mod. Phys.* **77** 137
[12] Hong H, Park H and Tang L 2007 *Phys. Rev.* E **76** 066104
[13] Arenas A, Díaz-Guilera A, Kurths J, Moreno Y and Zhou C 2008 *Phys. Rep.* **469** 93
[14] Qian Y, Huang X, Hu G and Liao X 2010 *Phys. Rev.* E **81** 036101
[15] Frame L and Simson M 1988 *Circulation* **78** 1277
[16] Courtemanche M, Glass L and Keener J P 1993 *Phys. Rev. Lett.* **70** 2182

[17] Grüner G *et al* 1989 *Charge Density Waves in Solids* vol 25 (Amsterdam: North-Holland)
[18] Rosenblum M, Pikovsky A and Kurths J 1997 *Phys. Rev. Lett.* **78** 4193
[19] Chenciner A and Montgomery R 2000 *Ann. Math.* **152** 881
[20] Braun O and Kivshar Y 2004 *The Frenkel–Kontorova Model: Concepts, Methods, and Applications* (New York: Springer)
[21] Aubry S and Le Daeron P 1983 *Physica* D **8** 381
[22] Bak P 1982 *Rep. Prog. Phys.* **45** 587
[23] Bär M and Eiswirth M 1993 *Phys. Rev.* E **48** R1635
[24] Ermentrout G and Kopell N 1986 *SIAM J. Appl. Math.* **46** 233
[25] Wiesenfeld K, Colet P and Strogatz S 1998 *Phys. Rev.* E **57** 1563
[26] Middleton A 1992 *Phys. Rev. Lett.* **68** 670
[27] Pietronero L and Strässler S 1983 *Phys. Rev.* B **28** 5863
[28] Matsukawa H and Takayama H 1984 *Solid State Commun.* **50** 283
[29] Strogatz S, Marcus C, Westervelt R and Mirollo R 1988 *Phys. Rev. Lett.* **61** 2380
[30] Verhulst F 1996 *Nonlinear Differential Equations and Dynamical Systems* (New York: Springer)
[31] Hale J K 1963 *Oscillations in Nonlinear Systems* (New York: McGraw-Hill)